Volume 59
Number 82
21 October 2023
Pages 12195–12356

ChemComm

Chemical Communications

rsc.li/chemcomm

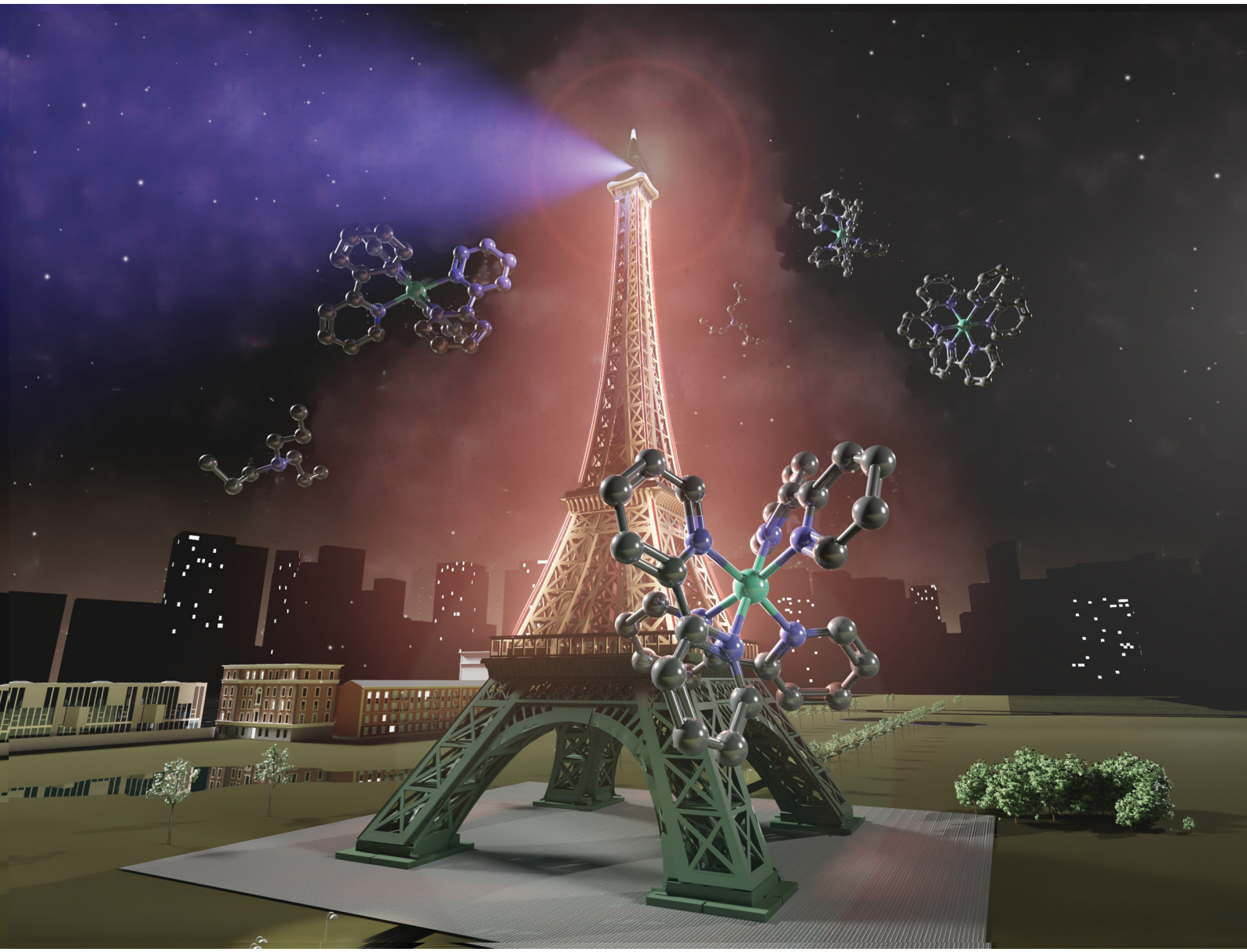

ISSN 1359-7345

ROYAL SOCIETY OF CHEMISTRY

COMMUNICATION

Gabriel Loget, Neso Sojic *et al.*

Local reactivity of metal–insulator–semiconductor photoanodes imaged by photoinduced electrochemiluminescence microscopy

ChemComm

COMMUNICATION

View Article Online
View Journal | View Issue

Cite this: *Chem. Commun.*, 2023, 59, 12262

Received 31st July 2023,
Accepted 18th September 2023

DOI: 10.1039/d3cc03702a

rsc.li/chemcomm

Local reactivity of metal–insulator–semiconductor photoanodes imaged by photoinduced electrochemiluminescence microscopy†

Julie Descamps,[a] Yiran Zhao,[b] Julie Le-Pouliquen,[c] Bertrand Goudeau,[a] Patrick Garrigue,[a] Karine Tavernier,[c] Yoan Léger,[c] Gabriel Loget *[bd] and Neso Sojic *[a]

Localized photoinduced electrochemiluminescence (PECL) is studied on photoanodes composed of Ir microbands deposited on n-Si/SiO_x. We demonstrate that PECL microscopy precisely imaged the hole-driven heterogeneous photoelectrochemical reactivity. The method is promising for elucidating the local activity of photoelectrodes that are employed in solar energy conversion.

Photoelectrochemistry of illuminated semiconductors is a field of research that deals with the charge transfer of photogenerated charge carriers (electrons and holes) at the solid–liquid interface.[1,2] It has promising applications in the field of energy conversion as the basis for artificial photosynthesis, in which solar energy is converted into H_2,[3,4] C1, or C2[5–7] products using water and/or CO_2 as reactants. In these systems, semiconductor photoelectrodes, often coated with protection and/or catalytic layers are immersed in a liquid electrolyte.[8–10] Upon light absorption, photogenerated charge carriers diffusing within the semiconductor, are collected at the catalyst and trigger redox reactions in the liquid phase. Photoelectrochemical characterization is mainly done by recording the current density (j) as a function of another parameter, for instance, the potential (E)/j (*i.e.*, voltammetry) or time (t)/j (*i.e.*, chronoamperometry) measurements, in which the j value corresponds to the faradaic charge transfer rate at the photoelectrode surface. Although these electroanalytical methods are straightforward for performance assessment, the j value only corresponds to the overall charge transfer rate, averaged over all the electrode surface, and does not allow for spatially-resolved determination of photoelectrochemical activity. However, probing the local activity is essential for elucidating the operation of photoelectrodes that are made by combining several materials, usually a semiconductor absorber, a protection layer, and a catalytic coating[7] (in the form of thin films[11,12] or particles[10,13–16] dispersed over the surface). Due to the complexity of these interfaces, the photoelectrochemical reaction is not expected to occur at the same rate over the whole surface. Visualizing local photoelectrochemical activity remains a challenge, which has been investigated by several groups[17] using different methods such as laser scanning techniques,[18] scanning electrochemical microscope variants,[19–24] or a combination of both.[25]

Electrochemiluminescence (ECL) is a light-emitting process initiated at an electrode surface.[26] The light originates from a luminophore molecule that is brought to its excited state by a highly exergonic electron-transfer reaction and relaxes to its ground state by emitting a photon.[27,28] This phenomenon is widely used for medical diagnosis applications and immunoassays,[29–36] with the ECL model system comprising tris(bipyridine)ruthenium(II) complex ($[Ru(bpy)_3]^{2+}$) and tri-*n*-propylamine (TPrA) as the luminophore and the co-reactant, respectively. Since ECL offers an optical readout, it has evolved progressively into a microscopy technique.[37–42] Single entities such as cells, bacteria, and organelles have been imaged by ECL with remarkable resolution.[39,43–49] Notably, ECL has also been employed for visualizing local electron transfer and catalytic activity of single nano-objects and particles.[50–55] Photoinduced ECL (PECL) combines semiconductor photoelectrochemistry and ECL.[56] In this process, a light input (λ_{exc}) is electrochemically converted and generates a light output (λ_{PECL}) through an ECL reaction. Depending on the choice of the electrode semiconductor material and the ECL system implied, PECL can allow either a downconversion ($\lambda_{PECL} < \lambda_{exc}$)[57] or an upconversion ($\lambda_{PECL} < \lambda_{exc}$) emission (Table S1, ESI†).[56,58–63] So far, PECL microscopy has been reported in two studies, and used to probe upconversion PECL at Au nanoparticles localized on Si

[a] *University of Bordeaux, Bordeaux INP, ISM, UMR CNRS 5255, Pessac 33607, France. E-mail: sojic@u-bordeaux.fr*
[b] *Univ Rennes, CNRS, ISCR (Institut des Sciences Chimiques de Rennes)-UMR6226, Rennes F-35000, France. E-mail: gabriel.loget@cnrs.fr*
[c] *Univ Rennes, INSA Rennes, CNRS, Institut FOTON-UMR 6082, F-35000, Rennes, France*
[d] *Institute of Energy and Climate Research, Fundamental Electrochemistry (IEK-9), Forschungszentrum Jülich GmbH, Jülich, 52425, Germany*

† Electronic supplementary information (ESI) available. See DOI: https://doi.org/10.1039/d3cc03702a

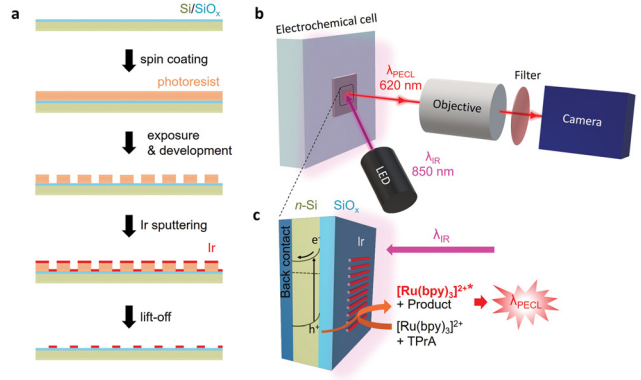

Fig. 1 (a) Scheme of the Ir microbands manufacturing on Si/SiO_x. (b) PECL microscopy imaging with IR incident light (λ_{exc} = 850 nm) from a LED and red PECL emission (λ_{PECL}) recorded by a camera. (c) Schematic representation of photoinduced holes generating PECL emission of $[Ru(bpy)_3]^{2+}$ with TPrA co-reactant at Ir microbands in PBS at pH 7.4.

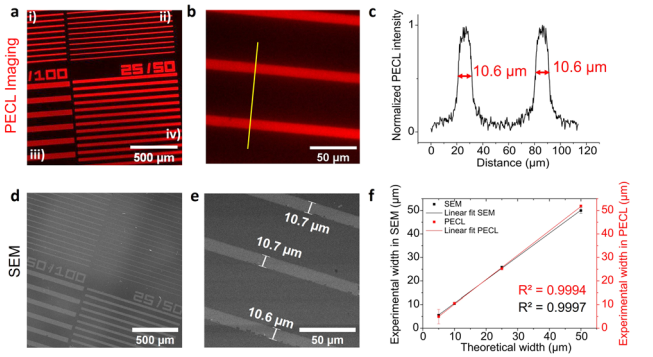

Fig. 2 (a) PECL imaging of n-Si/SiO_x patterned with Ir microbands of different width/pitch (i: 10/50 µm; ii: 5/50µm; iii: 50/100 µm and iv: 25/50 µm – the first and second values refer to the width and the pitch, respectively) at 0.8 V (*vs.* Ag/AgCl) in PBS 0.1 M solution (pH 7.4) containing 5 mM $[Ru(bpy)_3]^{2+}$ and 0.1 M TPrA. Exposure time t_{expo} = 1.5 s. (b) PECL images of the 10/50 µm microbands (as (i) in a) at a higher magnification. (c) Cross-section PECL intensity profiles extracted along the yellow line displayed in (b) with FWHM measurement of the patterns. (d) SEM picture of n-Si/SiO_x with Ir microbands as in (a). (e) Zoom on the 10 µm/50 µm microbands recorded by SEM. (f) Comparison of the microband width measured by SEM and PECL imaging (3 measurements for each point).

nanopillars[64] or TiO_2.[62] In these reports, PECL was triggered through the oxidation of luminol *via* photogenerated holes.

Herein, we report the detailed PECL microscopy study of inhomogeneous metal–insulator–semiconductor (MIS) photoanodes using the model $[Ru(bpy)_3]^{2+}$/TPrA system (Fig. 1). Such MIS-based architectures are often employed for manufacturing efficient and stable Si-based water-splitting photoanodes.[65–68] In particular, MIS photoanodes based on Si and Ir have been previously employed for photoelectrochemical water splitting[66,68–70] and it is known that n-Si/SiO_x/Ir photoanodes, in their homogeneous (*i.e.*, non-patterned) form exhibit exceptional PECL stability (Table S1, ESI†).[63] Here, inhomogeneous n-Si/SiO_x/Ir photoanodes are prepared by sputtering Ir microbands with a defined pattern. The operation of upconversion PECL and observation of the produced emission patterns allows resolving the solid/liquid photo-electrogenerated hole transfer at the local scale.

The MIS photoanodes were fabricated by chemical oxidation, photolithography and magnetron sputtering (Fig. S1, ESI†). First, Si/SiO_x was prepared by oxidizing a moderately doped photoactive n-Si surface to create a ≈1.5 nm-thick tunnel SiO_x layer, as described previously.[67,71] Prior to the PECL experiments, a 2 nm-thick Ir pattern (Fig. S2, ESI†) was deposited on Si/SiO_x using a lift-off process, described in Fig. 1a (see details in ESI†). Four types of Ir patterns with various width/pitch (50 µm/100 µm, 25 µm/50 µm, 10 µm/50 µm, and 5 µm/50 µm) were designed and produced. It is worth mentioning that the Si/SiO_x and the Si/SiO_x/Ir junctions were characterized by X-ray photoelectron spectroscopy and atomic force microscopy in a previous paper.[63] For the PECL microscopy experiments, the photoanode was excited by side-illumination with a near-IR LED (λ_{exc} = 850 nm) to photogenerate charge carriers, as shown in Fig. 1b and c. The localized PECL emission was imaged with a microscope equipped with an IR filter (Fig. S3, ESI†).

As shown in Fig. 2, microscopy images of PECL could be reliably recorded on n-Si/SiO_x/Ir under near-IR illumination at 0.8 V (all potential are here referred *vs.* Ag/AgCl) in the electrolytic solution containing both $[Ru(bpy)_3]^{2+}$ and TPrA. Fig. 2a shows that the red PECL light is homogeneously emitted over the Ir microbands, for all the patterns. At higher magnification (Fig. 2b), the PECL sharply delimits the contour of the Ir surface area allowing an excellent definition of the patterns, as further demonstrated by the intensity profile in Fig. 2c (*vide infra*). The bands made of Ir thin film are easily viewed by PECL because Ir acts as a collector for photogenerated charges and presents good charge transfer properties, leading to the efficient oxidation of both $[Ru(bpy)_3]^{2+}$ and TPrA producing light locally.[63]

In contrast, Si surface is passivated in the aqueous solution at the anodic potentials required for ECL generation. In other words, PECL is preferentially emitted at the Ir patterns (Fig. 2a and b). The 2 nm-thick Ir pattern was not observable with the naked eye or under a wide-field microscope, and therefore, scanning electron microscopy (SEM) was required to characterize the thin film patterns. Fig. 2d and e presents the SEM pictures of the Ir microbands that allow for a precise measurements of their dimensions. Then, we compared their dimensions measured by SEM and by PECL. For PECL microscopy, we extracted the PECL intensity profiles along a line perpendicular to the long band axis. More precisely, their full-width at half-maximum (FWHM) values were compared with the width measured by SEM for all the patterns: 10 µm/50 µm in Fig. 2c and, 50 µm/100 µm, 25 µm/50 µm, and 5 µm/50 µm in Fig. S4c, f and i, ESI†). In Fig. 2f, the PECL and SEM width measurements were plotted as a function of the theoretical width. The linear fits of both measurements show a slope close to 1 (R^2 = 0.9997 and R^2 = 0.9994 for the SEM and the PECL, respectively). This reveals the accuracy of the Ir pattern manufacturing with the lift-off process on one hand, and, on the other hand, that the PECL is restricted to the conductive patterns. We selected a

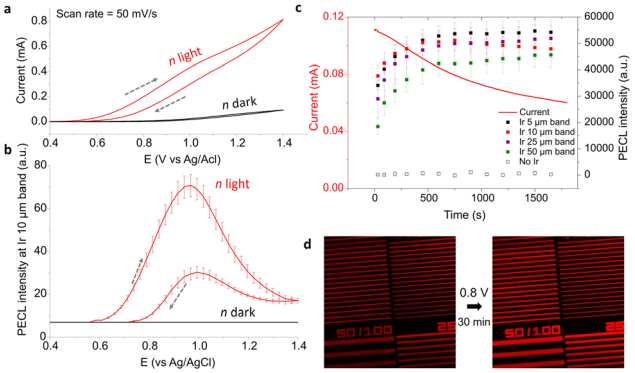

Fig. 3 (a) Voltammetric measurement of n-Si/SiO_x patterned with Ir microbands in the dark (black curve) and under LED illumination (red curve). The dashed grey arrows show the sweep direction. (b) Corresponding average PECL intensity of the 10 µm/50 µm Ir microbands under IR illumination (red curve) and in the dark (black curve). (c) Evolution of the current (line) and the PECL of each Ir band (squares) as a function of time at E_{app} = 0.8 V under LED light. (d) PECL imaging before (left) and after (right) a potentiostatic measurement. Same solution as in Fig. 2.

high concentration of TPrA (*i.e.* 0.1 M) for the PECL imaging experiments because (i) it generates a strong PECL signal and (ii) it confines the PECL-emitting layer at the electrode surface. Indeed, in the present experimental conditions, the size of the PECL reaction layer is typically ≈200 nm so much smaller than the dimensions of the bands.[72] Control experiments, presented in Fig. S5 (ESI†), were performed under illumination at open-circuit conditions to ensure that the observed pattern was not caused by reflection of the IR light. Furthermore, Fig. S5c (ESI†) shows that polarization of the electrode at 0.8 V in the dark did not lead to PECL emission, confirming the necessity of photocarrier generation in the PECL process.

We further investigated the photoelectrochemistry of the n-Si/SiO_x/Ir electrode. A cyclic voltammogram (CV) was recorded in the same electrolyte (5 mM $[Ru(bpy)_3]^{2+}$, 0.1 M TPrA, 0.1 M PBS at pH = 7.4) under IR illumination at λ_{exc} = 850 nm with a power density (P_{LED}) of 6.6 mW cm^{-2} (red curve) and in the dark (black curve, Fig. 3a). The PECL images were captured with the microscope at a speed of 2 frames per second (fps). In Fig. 3b, the corresponding average PECL intensity was plotted against the applied potential for the 10 µm/50 µm microbands. This points out that the local PECL emission was only initiated from +0.57 V. These measurements can be compared with that of an analogous but non-photoactive p^{++}-Si/SiO_x/Ir MIS anode prepared on a highly-doped, degenerate p^{++}-Si surface and studied in the dark. Indeed, ECL microscopy on these anodes revealed that they also promote local ECL at the Ir/electrolyte interface, however, at higher potentials than that required for their illuminated photoactive counterpart (n-Si/SiO_x/Ir). This shift of ECL onset potential can be clearly observed in Fig. S6a (ESI†) where the CV obtained for p^{++}-Si/SiO_x/Ir and n-Si/SiO_x/Ir under different illumination conditions are plotted together. This shift of onset potential (here ≈0.5 V) is characteristic of a conventional photoanode behavior and caused by the generation of a photovoltage, this was already observed (to a lower extent) on non-patterned n-Si/SiO_x/Ir photoanodes.[63,73]

We then studied the evolution of PECL on the illuminated n-Si/SiO_x/Ir over time by potentiostatic measurement at 0.8 V for 30 min while capturing microscopy pictures. The PECL intensity averages were measured on the pictures for the 50 µm/100 µm, 25 µm/50 µm, 10 µm/50 µm, and 5 µm/50 µm microbands. On Fig. 3c, it can be observed that the photocurrent decreases by −45% after 30 min, but, meanwhile, the PECL intensities increased and reached a plateau after about 10 min. The pictures at the beginning and at the end of the potentiostatic measurement, (recorded with the same conditions of the CCD camera with t_{expo} = 0.5 s) complete this observation with a PECL that appears more intense at the end of the experiment (Fig. 3d). This behavior could be explained by the anodic passivation of the Si/SiO_x surface that inhibits the flow of residual current onto the Ir-free area and the surface oxidation of Ir that could influence the ECL process. However, the pattern remains identical after 30 min, showing no obvious damage of the patterns. In addition to the PECL on n-Si/SiO_x/Ir, the ECL intensity on the p^{++}-Si/SiO_x/Ir electrode was also recorded (in the dark at 1.2 V, Fig. S6b and S7, ESI†), confirming our observations.

To conclude, we have performed a PECL microscopy study of MIS n-Si/SiO_x/Ir microbands. This junction has been considered so far as the most stable interface for manufacturing PECL photoanodes (Table S1, ESI†)[63] and has implications in the field of photoelectrochemical solar energy conversion.[66,68–70] Inhomogeneous photoactive surfaces comprising ultrathin Ir microbands were prepared on Si/SiO_x and studied under an optical microscope by PECL under IR irradiation (λ_{exc} = 850 nm). The emission patterns (λ_{PECL} = 635 nm) were intense, stable, and presented geometrical features identical to that of the Ir microbands. These results clearly revealed, in the form of a snapshot, that photoelectrochemical charge transfer occurs at the surface Ir microbands and is inhibited at the SiO_x surface. We anticipate that PECL microscopy can be used as a novel approach for understanding the complexity of inhomogeneous solid/liquid junctions and could help the further development in photoelectrochemical solar energy conversion.

The manuscript was written through contributions of all authors. This work was funded by ANR (LiCORN, ANR-20-CE29-0006).

Conflicts of interest

There are no conflicts to declare.

References

1 H. Gerischer, in *Solar Energy Conversion*, ed. B. O. Seraphin, Springer, Heidelberg, Berlin, 1979, pp. 115–172.
2 M. X. Tan, P. E. Laibinis, S. T. Nguyen, J. M. Kesselman, C. E. Stanton and N. S. Lewis, in *Progress in Inorganic Chemistry*, ed. K. D. Karlin, John Wiley & Sons, Inc., Hoboken, USA, 2007.
3 M. G. Walter, E. L. Warren, J. R. McKone, S. W. Boettcher, Q. Mi, E. A. Santori and N. S. Lewis, *Chem. Rev.*, 2010, **110**, 6446.
4 D. G. Nocera, *Acc. Chem. Res.*, 2012, **45**, 767–776.
5 T. Morikawa, S. Sato, K. Sekizawa, T. M. Suzuki and T. Arai, *Acc. Chem. Res.*, 2022, **55**, 933–943.

6 P. B. Pati, R. Wang, E. Boutin, S. Diring, S. Jobic, N. Barreau, F. Odobel and M. Robert, *Nat. Commun.*, 2020, **11**, 3499.
7 I. Roh, S. Yu, C.-K. Lin, S. Louisia, S. Cestellos-Blanco and P. Yang, *J. Am. Chem. Soc.*, 2022, **144**, 8002–8006.
8 D. Bae, B. Seger, P. C. K. Vesborg, O. Hansen and I. Chorkendorff, *Chem. Soc. Rev.*, 2017, **46**, 1933–1954.
9 G. Loget, *Curr. Opin. Colloid Interface Sci.*, 2019, **39**, 40–50.
10 B. Fabre and G. Loget, *Acc. Mater. Res.*, 2023, **4**, 133–142.
11 L. Pan, J. H. Kim, M. T. Mayer, M.-K. Son, A. Ummadisingu, J. S. Lee, A. Hagfeldt, J. Luo and M. Grätzel, *Nat. Catal.*, 2018, **1**, 412.
12 I. A. Digdaya, G. W. P. Adhyaksa, B. J. Trześniewski, E. C. Garnett and W. A. Smith, *Nat. Commun.*, 2017, **8**, 15968.
13 F. A. L. Laskowski, S. Z. Oener, M. R. Nellist, A. M. Gordon, D. C. Bain, J. L. Fehrs and S. W. Boettcher, *Nat. Mater.*, 2020, **19**, 69.
14 G. Loget, B. Fabre, S. Fryars, C. Mériadec and S. Ababou-Girard, *ACS Energy Lett.*, 2017, **2**, 569–573.
15 K. Oh, V. Dorcet, B. Fabre and G. Loget, *Adv. Energy Mater.*, 2020, **10**, 1902963.
16 S. Lee, L. Ji, A. C. De Palma and E. T. Yu, *Nat. Commun.*, 2021, **12**, 3982.
17 D. V. Esposito, J. B. Baxter, J. John, N. S. Lewis, T. P. Moffat, T. Ogitsu, G. D. O'Neil, T. A. Pham, A. A. Talin, J. M. Velazquez and B. C. Wood, *Energy Environ. Sci.*, 2015, **8**, 2863–2885.
18 G. Loget, S. So, R. Hahn and P. Schmuki, *J. Mater. Chem. A*, 2014, **2**, 17740–17745.
19 J. Lee, H. Ye, S. Pan and A. J. Bard, *Anal. Chem.*, 2008, **80**, 7445–7450.
20 B. D. B. Aaronson, J. C. Byers, A. W. Colburn, K. McKelvey and P. R. Unwin, *Anal. Chem.*, 2015, **87**, 4129–4133.
21 V. Badets, G. Loget, P. Garrigue, N. Sojic and D. Zigah, *Electrochim. Acta*, 2016, **222**, 84–91.
22 F. Gelb, Y.-C. Chueh, N. Sojic, V. Keller, D. Zigah and T. Cottineau, *Sustain. Energy Fuels*, 2020, **4**, 1099–1104.
23 R. Gutkowski, C. Khare, F. Conzuelo, Y. U. Kayran, A. Ludwig and W. Schuhmann, *Energy Environ. Sci.*, 2017, **10**, 1213–1221.
24 X. Zhou, Z. T. Gossage, B. H. Simpson, J. Hui, Z. J. Barton and J. Rodríguez-López, *ACS Nano*, 2016, **10**, 9346–9352.
25 D. V. Esposito, I. Levin, T. P. Moffat and A. A. Talin, *Nat. Mater.*, 2013, **12**, 562–568.
26 Z. Liu, W. Qi and G. Xu, *Chem. Soc. Rev.*, 2015, **44**, 3117–3142.
27 W. Miao and J.-P. Choi, in *Electrogenerated chemiluminescence* ed. A. J. Bard, Marcel Dekker, New York, 2004, pp. 213–271.
28 *Analytical Electrogenerated Chemiluminescence*, ed. N. Sojic, RSC Publishing, Cambridge, 2020.
29 F. Du, Y. Chen, C. Meng, B. Lou, W. Zhang and G. Xu, *Curr. Opin. Electrochem.*, 2021, **28**, 100725.
30 A. Zanut, A. Fiorani, S. Canola, T. Saito, N. Ziebart, S. Rapino, S. Rebeccani, A. Barbon, T. Irie, H.-P. Josel, F. Negri, M. Marcaccio, M. Windfuhr, K. Imai, G. Valenti and F. Paolucci, *Nat. Commun.*, 2020, **11**, 2668.
31 M. Guo, D. Du, J. Wang, Y. Ma, D. Yang, M. A. Haghighatbin, J. Shu, W. Nie, R. Zhang, Z. Bian, L. Wang, Z. J. Smith and H. Cui, *Chem. Biomed. Imaging*, 2023, **1**, 179–185.
32 Y. Wang, J. Ding, P. Zhou, J. Liu, Z. Qiao, K. Yu, J. Jiang and B. Su, *Angew. Chem., Int. Ed.*, 2023, **62**, e202216525.
33 E. Faatz, A. Finke, H.-P. Josel, G. Prencipe, S. Quint and M. Windfuhr, *Analytical Electrogenerated Chemiluminescence*, RSC, Cambridge, 2020, pp. 443–470.
34 X. Yang, J. Hang, W. Qu, Y. Wang, L. Wang, P. Zhou, H. Ding, B. Su, J. Lei, W. Guo and Z. Dai, *J. Am. Chem. Soc.*, 2023, **145**, 16026–16036.
35 F. Deiss, C. N. LaFratta, M. Symer, T. M. Blicharz, N. Sojic and D. R. Walt, *J. Am. Chem. Soc.*, 2009, **131**, 6088–6089.
36 H. Qi and C. Zhang, *Anal. Chem.*, 2020, **92**, 524–534.
37 A. Zanut, A. Fiorani, S. Rebeccani, S. Kesarkar and G. Valenti, *Anal. Bioanal. Chem.*, 2019, **411**, 4375–4382.
38 J. Zhang, S. Arbault, N. Sojic and D. Jiang, *Ann. Rev. Anal. Chem.*, 2019, **12**, 275–295.
39 J. Dong, Y. Lu, Y. Xu, F. Chen, J. Yang, Y. Chen and J. Feng, *Nature*, 2021, **596**, 244–249.
40 X. Gou, Z. Xing, C. Ma and J.-J. Zhu, *Chem. Biomed. Imaging*, 2023, **1**, 414–433.
41 S. Rebeccani, A. Zanut, C. I. Santo, G. Valenti and F. Paolucci, *Anal. Chem.*, 2022, **94**, 336–348.
42 L. Ding, P. Zhou, Y. Yan and B. Su, *Chem. Biomed. Imaging*, 2023, DOI: 10.1021/cbmi.3c00066.
43 Y. Ma, C. Colin, J. Descamps, S. Arbault and N. Sojic, *Angew. Chem., Int. Ed.*, 2021, **60**, 18742–18749.
44 H. Gao, W. Han, H. Qi, Q. Gao and C. Zhang, *Anal. Chem.*, 2020, **92**, 8278–8284.
45 W. Zhao, H.-Y. Chen and J.-J. Xu, *Chem. Sci.*, 2021, **12**, 5720–5736.
46 H. Ding, P. Zhou, W. Fu, L. Ding, W. Guo and B. Su, *Angew. Chem., Int. Ed.*, 2021, **60**, 11769–11773.
47 Y. Zhou, J. Dong, P. Zhao, J. Zhang, M. Zheng and J. Feng, *J. Am. Chem. Soc.*, 2023, **145**, 8947–8953.
48 Y. Wang, W. Guo, Q. Yang and B. Su, *J. Am. Chem. Soc.*, 2020, **142**, 1222–1226.
49 J. Descamps, C. Colin, G. Tessier, S. Arbault and N. Sojic, *Angew. Chem., Int. Ed.*, 2023, **135**, e202218574.
50 J. Dong, Y. Xu, Z. Zhang and J. Feng, *Angew. Chem., Int. Ed.*, 2022, **61**, e202200187.
51 M.-M. Chen, C.-H. Xu, W. Zhao, H.-Y. Chen and J.-J. Xu, *J. Am. Chem. Soc.*, 2021, **143**, 18511–18518.
52 M.-J. Zhu, J.-B. Pan, Z.-Q. Wu, X.-Y. Gao, W. Zhao, X.-H. Xia, J.-J. Xu and H.-Y. Chen, *Angew. Chem., Int. Ed.*, 2018, **130**, 4074–4078.
53 Y. Lu, X. Huang, S. Wang, B. Li and B. Liu, *ACS Nano*, 2023, **17**, 3809–3817.
54 K. Wu, R. Chen, Z. Zhou, X. Chen, Y. Lv, J. Ma, Y. Shen, S. Liu and Y. Zhang, *Angew. Chem., Int. Ed.*, 2023, **135**, e202217078.
55 X. Hu, S. Yu, C. Wang, X. Zhang, J. Pan and H. Ju, *Anal. Chem.*, 2023, **95**, 4496–4502.
56 Y. Zhao, L. Bouffier, G. Xu, G. Loget and N. Sojic, *Chem. Sci.*, 2022, **13**, 2528–2550.
57 J. Yu, H. Saada, R. Abdallah, G. Loget and N. Sojic, *Angew. Chem., Int. Ed.*, 2020, **132**, 15269–15272.
58 Y. Zhao, J. Descamps, Y. Léger, L. Santinacci, S. Zanna, N. Sojic and G. Loget, *Electrochim. Acta*, 2023, **444**, 142013.
59 D. Laser and A. J. Bard, *Chem. Phys. Lett.*, 1975, **34**, 6.
60 Y. B. Vogel, N. Darwish and S. Ciampi, *Cell Rep. Phys. Sci.*, 2020, **1**, 100107.
61 Y. Zhao, J. Yu, G. Xu, N. Sojic and G. Loget, *J. Am. Chem. Soc.*, 2019, **141**, 13013–13016.
62 J.-W. Xue, C.-H. Xu, W. Zhao, H.-Y. Chen and J.-J. Xu, *Nano Lett.*, 2023, **23**, 4572–4578.
63 Y. Zhao, J. Descamps, S. Ababou-Girard, J.-F. Bergamini, L. Santinacci, Y. Léger, N. Sojic and G. Loget, *Angew. Chem., Int. Ed.*, 2022, **61**, e20220186.
64 Y. Zhao, J. Descamps, N. H. Al Bast, M. Duque, J. Esteve, B. Sepulveda, G. Loget and N. Sojic, *J. Am. Chem. Soc.*, 2023, **145**, 17420–17426.
65 S. Hu, M. R. Shaner, J. A. Beardslee, M. Lichterman, B. S. Brunschwig and N. S. Lewis, *Science*, 2014, **344**, 1005–1009.
66 A. G. Scheuermann, J. P. Lawrence, K. W. Kemp, T. Ito, A. Walsh, C. E. D. Chidsey, P. K. Hurley and P. C. McIntyre, *Nat. Mater.*, 2016, **15**, 99–105.
67 G. Loget, C. Mériadec, V. Dorcet, B. Fabre, A. Vacher, S. Fryars and S. Ababou-Girard, *Nat. Commun.*, 2019, **10**, 3522.
68 S. E. Jun, Y.-H. Kim, J. Kim, W. S. Cheon, S. Choi, J. Yang, H. Park, H. Lee, S. H. Park, K. C. Kwon, J. Moon, S.-H. Kim and H. W. Jang, *Nat. Commun.*, 2023, **14**, 609.
69 O. L. Hendricks, R. Tang-Kong, A. S. Babadi, P. C. McIntyre and C. E. D. Chidsey, *Chem. Mater.*, 2019, **31**, 90–100.
70 M. Ben-Naim, D. W. Palm, A. L. Strickler, A. C. Nielander, J. Sanchez, L. A. King, D. C. Higgins and T. F. Jaramillo, *ACS Appl. Mater. Interfaces*, 2020, **12**, 5901–5908.
71 J. Dabboussi, R. Abdallah, L. Santinacci, S. Zanna, A. Vacher, V. Dorcet, S. Fryars, D. Floner and G. Loget, *J. Mater. Chem. A*, 2022, **10**, 19769–19776.
72 A. Chovin, P. Garrigue, P. Vinatier and N. Sojic, *Anal. Chem.*, 2004, **76**, 357–364.
73 Y. Zhao, J. Descamps, B. Le Corre, Y. Léger, A. Kuhn, N. Sojic and G. Loget, *J. Phys. Chem. Lett.*, 2022, **13**, 5538–5544.